ADVANCED FUNCTIONAL MATERIALS
www.afm-journal.de

Materials Views
www.MaterialsViews.com

Synthesis of Au–CdS Core–Shell Hetero-Nanorods with Efficient Exciton–Plasmon Interactions

Min Li, Xue-Feng Yu, Shan Liang, Xiao-Niu Peng, Zhong-Jian Yang, Ya-Lan Wang, and Qu-Quan Wang**

The synthesis of large lattice mismatch metal-semiconductor core–shell hetero-nanostructures remains challenging, and thus the corresponding optical properties are seldom discussed. Here, we report the gold-nanorod-seeded growth of Au–CdS core–shell hetero-nanorods by employing Ag_2S as an interim layer that favors CdS shell formation through a cation-exchange process, and the subsequent CdS growth, which can form complete core–shell structures with controllable shell thickness. Exciton–plasmon interactions observed in the Au–CdS nanorods induce shell thickness-tailored and red-shifted longitudinal surface plasmon resonance and quenched CdS luminescence under ultraviolet light excitation. Furthermore, the Au–CdS nanorods demonstrate an enhanced and plasmon-governed two-photon luminescence under near-infrared pulsed laser excitation. The approach has potential for the preparation of other metal-semiconductor hetero-nanomaterials with complete core–shell structures, and these Au–CdS nanorods may open up intriguing new possibilities at the interface of optics and electronics.

1. Introduction

A key goal in nanomaterial research has been the integration of different materials within the same structure so that multiple functionalities may be incorporated.[1] Promising examples of such structures are metal-semiconductor nanocomposites that have attracted increasing attention because of their optical properties,[2,3] photocatalytic activities,[4] and ultrafast carrier dynamics.[5,6] Understanding these systems is important for the future development of electronic and photonic devices.[1] Furthermore, the interactions between the nanoscale-spaced metal and semiconductor components can greatly improve the overall application performance of the nanocomposites and can even generate new synergetic properties.[7,8] For example, in metal-semiconductor nanostructures, metallic ingredients can increase the photocatalytic and light-harvesting efficiencies of semiconductors by improving the charge separation[4,9,10] and by enhancing the light absorption.[11,12] Metallic components can also alter the photoluminescence (PL) behavior of semiconductors[13–16] and can modify their nonlinear optical response.[12,17] Such metal-based core–shell structures with a high shell refractive index can support enhanced electromagnetic fields[18–20] and may find applications in surface-enhanced Raman scattering (SERS)[20] and surface fluorescence enhancement.[13] Furthermore, the coupling of a semiconductor with metal components allows the plasmonic modes of the latter to be excited and controlled for energy transmission studies.[21,22]

The synthesis of metal-semiconductor hetero-nanostructures with positional and morphological control still remains a challenge because of the large lattice mismatch between the two components. The pursuit of the formation of such nanocomposites is driven not only by the aesthetics of the products but also by the potentially enhanced integrated functions.[1–3,8,23–31] Most previous efforts have been focused on the synthesis of metal-semiconductor nanocomposites, and the general methods used included the selective growth of metals onto the tips and surfaces of semiconductor nanocrystals,[9,14] the diffusion of metals into semiconductors, and the growth of semiconductors on metal seeds.[3,5,8,11,25,26] Moreover, the synthesis of metal-semiconductor core–shell nanostructures has aroused special interest because the core–shell geometry can maximize the interfacial area and thus provide an excellent platform for studying the exciton-plasmon interactions and promote effective energy transfer to favor subsequent optical responses.[8] Talapin et al. established a method of using Pb-oleate complexes to form PbS shells on oil-dispersible gold nanospheres.[11] Hsu et al. successfully prepared water-dispersible Au–CdS core–shell nanospheres by binding L-cysteine-Cd^{2+} complexes to Au nanospheres.[25] Wang's group synthesized various Au–metal sulfide core–shell nanostructures by binding metal thiobenzoates onto differently shaped gold structures.[8] These methods relied on special organic metal precursors for hetero-growth. On the other hand, Alivisatos's group established a cation-exchange technology that provided a novel route for converting one crystalline solid into another.[32] This method was very recently used to synthesize oil-soluble gold-semiconductor core–shell nanospheres through a nonepitaxial growth process.[26]

Dr. M. Li, X.-F. Yu, S. Liang, X.-N. Peng, Z.-J. Yang, Y.-L. Wang, Prof. Q.-Q. Wang
Department of Physics
Key Laboratory of Artificial
Micro- and Nano-structures of the Ministry of Education
and School of Physics and Technology
Wuhan University, Wuhan 430072, P. R. China
E-mail: yxf@whu.edu.cn; qqwang@whu.edu.cn

DOI: 10.1002/adfm.201002233

One remarkable feature of novel metal nanoparticles is the degree to which their optical properties can be tuned through changes in their shape and morphology.[33] Compared with more symmetrically shaped nanoparticles (such as nanospheres), gold nanorods offer a means of tailoring the longitudinal surface plasmon resonance (LSPR) wavelength to the near-infrared (NIR) region with significant advantages.[34] For example, the sensitivity of the LSPR bands to the local environment is quite important for chemical and biological sensing.[35] Radiative elastic Rayleigh scattering, inelastic Raman scattering, and two-photon induced luminescence offer multiple modalities for detection and imaging.[36–41] Furthermore, nanorods can assemble into aligned configurations and thus give rise to optical anisotropies that prove useful to potential photonic devices.[41] The most-successful known methods for gold nanorod synthesis rely on the use of the cationic surfactant cetyltrimethylammonium bromide (CTAB) as the "shape-inducing" agent.[42–44] The particular micellar environment enhances nanorod stability under aggressive conditions, such as centrifugation and high ionic strength.[44] However, the strong and anisotropic binding of CTAB molecules to the gold surface makes it more difficult to form hybrid shells compared to other synthetic protocols.[44] Therefore, when using gold nanorods as cores to synthesize metal-semiconductor composites, only special metal-chalcogenides (such as Au–Ag_2S)[8] with a good lattice match ever form complete shells. To date, it remains a great challenge to obtain metal-semiconductor core–shell nanostructures with gold nanorods, and thus the corresponding optical research is scarce.

In this paper, a method for obtaining Au–CdS core–shell nanostructures is established by using CTAB-capped gold nanorods as seeds. This strategy relies on the pre-growth of Ag_2S as an interim layer that favors CdS shell formation through a cation-exchange process, and thus the subsequent CdS growth can lead to complete Au–CdS core–shell nanostructures with controllable shell thickness. The Au–CdS nanorods demonstrate shell thickness-tailored LSPR wavelengths, Au-quenched exciton luminescence, and CdS-enhanced Au two-photon PL under NIR laser excitation.

2. Results and Discussion

2.1. Synthesis Protocols and Sample Structures

The steps of the synthesis protocol are outlined in **Figure 1**, and each growth stage is characterized in detail by the transmission electron microscopy (TEM) images in **Figure 2**. Au–CdS is a typical example to illustrate the proposed mechanism for metal-semiconductor core–shell structures, in which the lattice mismatch between the two majority lattice planes of bulk Au and CdS is up to 43%.[26] The average diameter and length of the Au nanorods used are 17 ± 2 nm and 61 ± 6 nm, respectively (see Figure 2a). The proposed growth mechanism can be qualitatively understood on the basis of thermodynamics and the coordination chemistry of the ionic transformation involved in the growth reactions.[26] The key to this method relies on the synthesis of Ag_2S layers to achieve the hetero-growth of CdS on the original gold nanorods. The growth progress can be summarized in three steps:

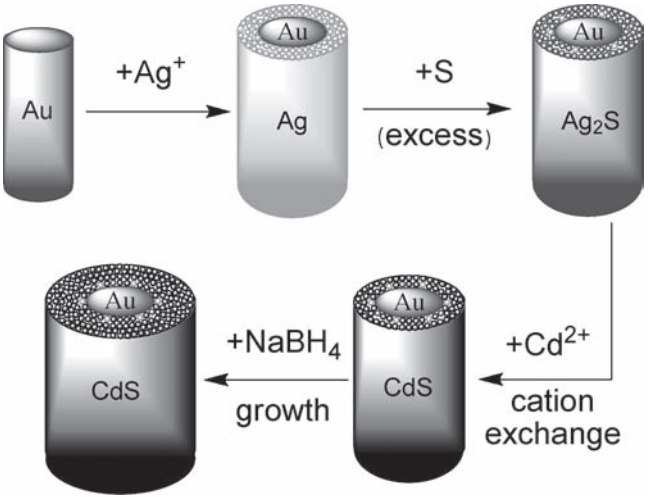

Figure 1. Growth scheme of Au–CdS core–shell nanorods.

1) Ag shell growth. First, the silver shell is easily grown on the gold nanorods because of the perfect match of the lattice constants of the two metals. As shown in Figure 2b, an anisotropic silver coating occurred in this synthesis, which resulted in a shuttle-like shape for the Au–Ag nanorods.[45]
2) Ag_2S shell growth. Because the electronegativity of Ag is similar to that of many anions X (such as chalcogenides, As, and P), the Ag shells can easily be modified to form silver compound shells (Ag_2X).[3,8,26,27] In our synthesis, the Ag_2S shells were obtained by adding excess sulfur in the growth solution containing Au–Ag nanorods (see Figure 2c).
3) CdS shell growth. It has been demonstrated that cation exchange represents a versatile route for converting one crystalline solid into another.[32] In the proposed synthesis, this process was harnessed to convert Ag_2S to CdS by adding a certain amount of $Cd(NO_3)_2$ to the growth solution. Then, the excess Cd^{2+} ions reacted with the residual sulfur in the solution for further growth of the CdS shells. Such growth could be accelerated by adding $NaBH_4$. As shown in Figure 2d–f, the final Au–CdS products had complete core–shell structures, and the shell thickness could be controlled from about 4.5 to 15.0 nm by regulating the molar ratio of Cd/Au in the reaction solution.

We note that the first step of Ag shell formation plays an important role in our synthesis route. If the Au–CdS samples were synthesized without this step, the final products would be irregular aggregates. Furthermore, the thickness of the Ag shells could be regulated within several nanometers by changing the $AgNO_3$ amount.[45,46] However, the difficulty in accurately identifying the Au–Ag interface prevents us from measuring the Ag shell thickness quantitatively.[46] The Au–Ag nanorods exhibited in Figure 2b were obtained by using 2.5 μL of $AgNO_3$. When 16 μL of $AgNO_3$ was used, the Ag shell thickness increased, and thicker Ag_2S shells (ca. 4.5 nm) were obtained in the next step. However, the thickness of the final CdS shells was only influenced slightly (see Figure S1 in the Supporting Information for

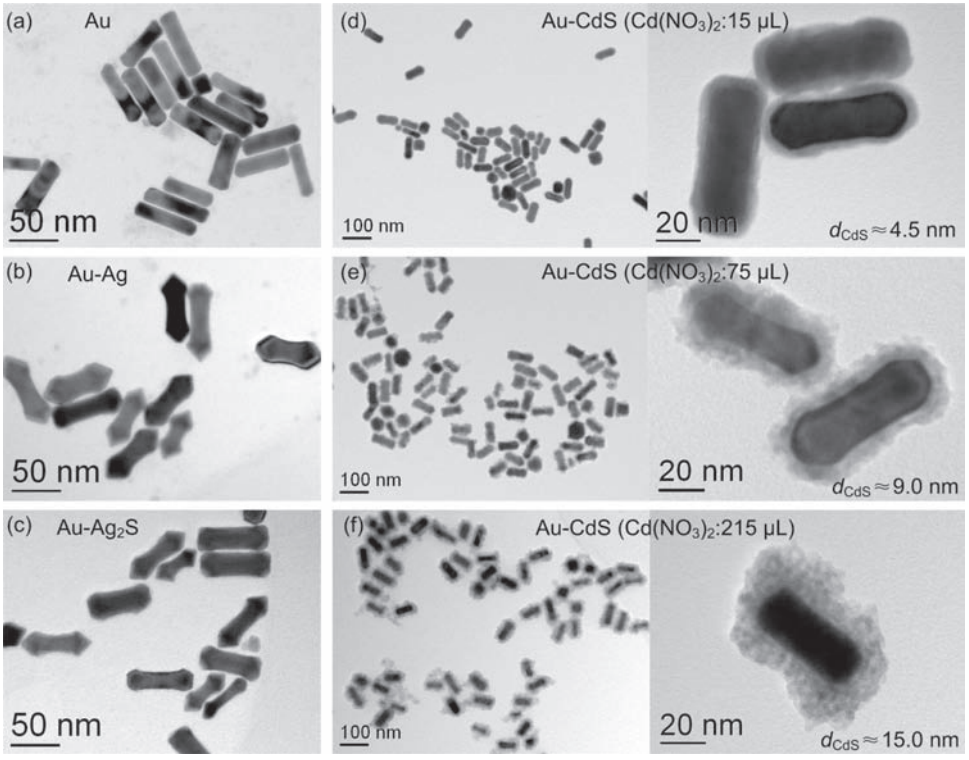

Figure 2. a–c) TEM images of original Au nanorods (a) and intermediate products of Au–Ag (b) and Au–Ag_2S (c) core–shell nanorods. d–f) Low (left) and high (right) magnitude TEM images of final products of Au–CdS core–shell nanorods with CdS shell thickness (d_{CdS}) of around 4.5 nm (d), 9.0 nm (e), and 15.0 nm (f).

details). Some byproducts of Ag nanoparticles were synthesized when even more $AgNO_3$ was used.

Figure 3 shows the detailed crystallographic structures and composites of the as-obtained Au–CdS core–shell nanorods. A high-resolution TEM (HRTEM) image was taken at the interface of the core and shell regions of a single Au–CdS particle. Two distinct sets of lattice fringes appeared. An interlayer spacing of 0.24 nm was obtained in the core region, which was in good agreement with the *d* spacing of the (111) lattice planes of the fcc gold crystal.[8] In the shell region, an interlayer spacing of 0.34 nm was observed, which complies with the lattice spacing of the (002) planes of CdS[25] and was confirmed by the corresponding fast-Fourier transform (FFT) pattern (inset in Figure 3a). To confirm the composition of the samples further, energy-dispersive X-ray (EDX) analysis was performed on an individual nanocrystal. The spectrum in Figure 3b shows strong Au, Cd, and S peaks in addition to the C, O, and Cu peaks generated by the copper grid. This result indicates the presence of Au, Cd, and S elements in the core–shell nanostructures. A faint Ag peak also appeared in the spectrum, indicating some residual Ag in the core–shell structures.

In brief, the proposed synthesis relies on the use of cation-exchangeable Ag_2S layers to overcome the limitation of the lattice mismatch between gold and CdS for hetero-growth. The merits of this method include well-defined and complete shell morphologies, easily controllable shell thickness, and monodispersed final products with few CdS byproducts (see Figure S2 for one typical TEM image containing a great number of Au–CdS nanorods with few CdS byproducts). This method to synthesize Au–CdS nanorods can be readily extended to synthesize other gold-metal sulfide core–shell nanocrystals. For example, Figure S3 in the Supporting Information shows a TEM image of Au–ZnS core–shell nanorods that were synthesized by using the same protocol except using $Zn(NO_3)_2$ instead of $Cd(NO_3)_2$. Furthermore, the use of pre-grown gold nanocrystals as seeds for the synthesis allows their shapes and sizes to be chosen rationally. Thus, this strategy can easily be extended to other gold-semiconductor nanocrystals by employing differently shaped gold nanocrystals, such as nanospheres, nanopolyhedras, and nanocubes. For example, TEM images of Au–CdS core–shell nanospheres are shown in Figure S4 of the Supporting Information.

2.2. Tuning of Surface Plasmon Resonance

The fine tuning of the shells on the Au nanorods could be monitored by the solution output color and LSPR wavelengths of the core–shell nanorods (see **Figure 4**). The original gold nanorod LSPR appeared at around 790 nm, and the transverse SPR (TSPR) band was centered at about 520 nm. Both the LSPR and TSPR wavelengths of the Au–Ag nanorods blue-shifted with the silver coating,[45] and the corresponding solution color changed from pink to deep yellow. After the Ag_2S layers were formed,

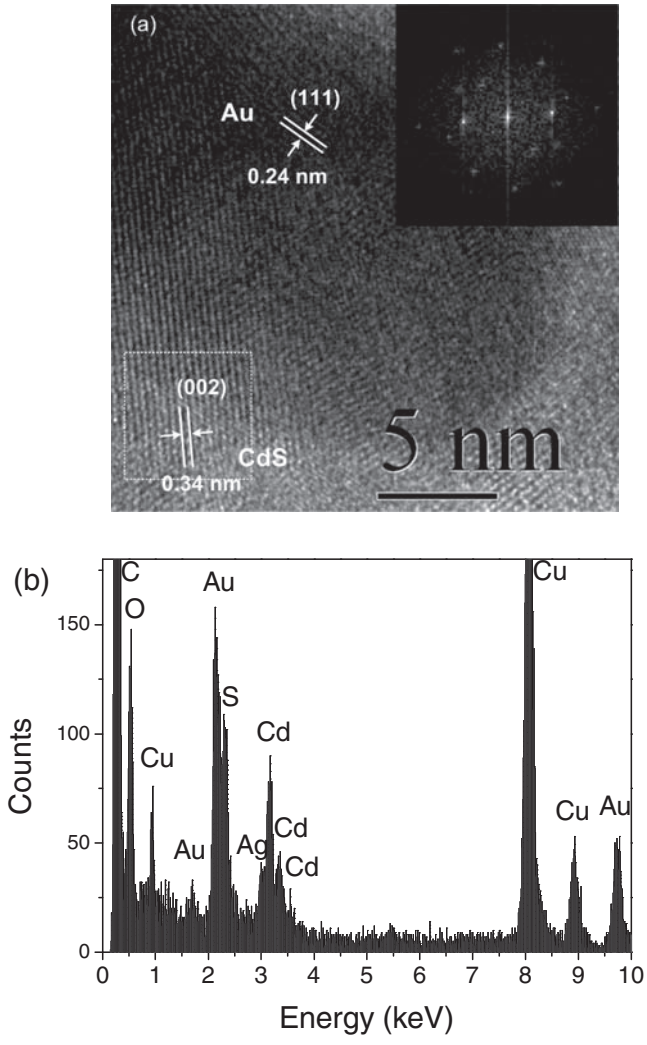

Figure 3. a) HRTEM and b) corresponding EDX analysis spectrum of an individual Au–CdS core–shell nanorod. The inset in (a) shows the FFT pattern of the indicated square area in the image.

the SPR wavelengths red-shifted because of the increase in the refractive index of the surrounding medium,[8] and the solution color changed to purple-brown. Finally, for the Au–CdS core–shell nanorods with a shell thickness of about 15.0 nm, the LSPR wavelengths red-shifted to about 868 nm, and the corresponding solution color changed to blue.

The unique characteristics of the core–shell geometry enable a continuous tuning of the plasmonic resonance by controlling the thickness of the CdS shell created around the Au nanorods (see **Figure 5**). When the CdS shell thickness increases, a pronounced red-shift in the LSPR peak wavelength can be observed, and both the TSPR and the LSPR bands broaden slightly. The characteristic CdS absorption band at around 445 nm can also be found in the spectra when the CdS shells are thicker than 9.0 nm. However, the spectra are obviously not a simple sum of both components. Instead, these results reflect the coupling of the excitonic state to the plasmonic mode of the gold nanorods, which exhibits broadening and red-shift effects of the SPR bands.

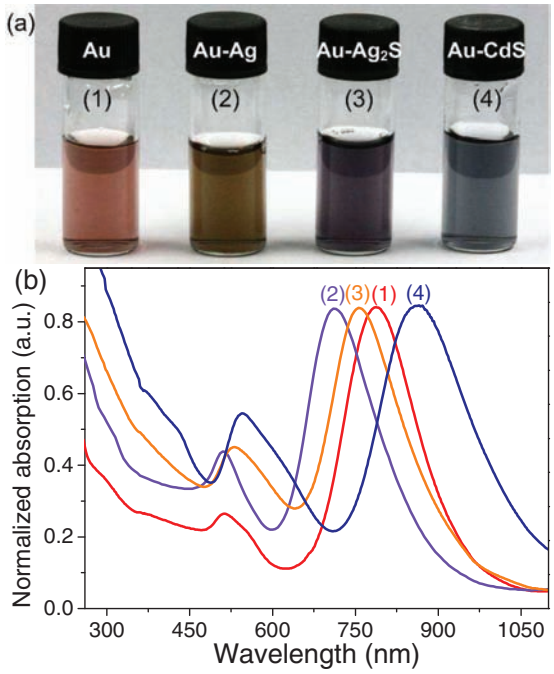

Figure 4. a) Digital photographs and b) normalized absorption spectra of 1) Au, 2) Au–Ag, 3) Au–Ag_2S, and 4) Au–CdS nanorods.

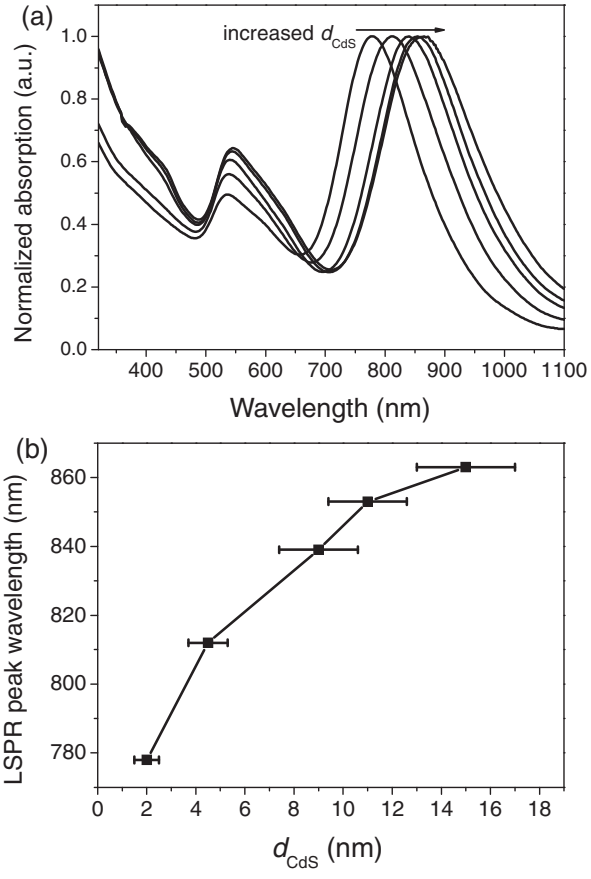

Figure 5. a) Normalized absorption spectra of Au–CdS core–shell nanorods with increased d_{CdS}. b) LSPR peak wavelength versus d_{CdS}.

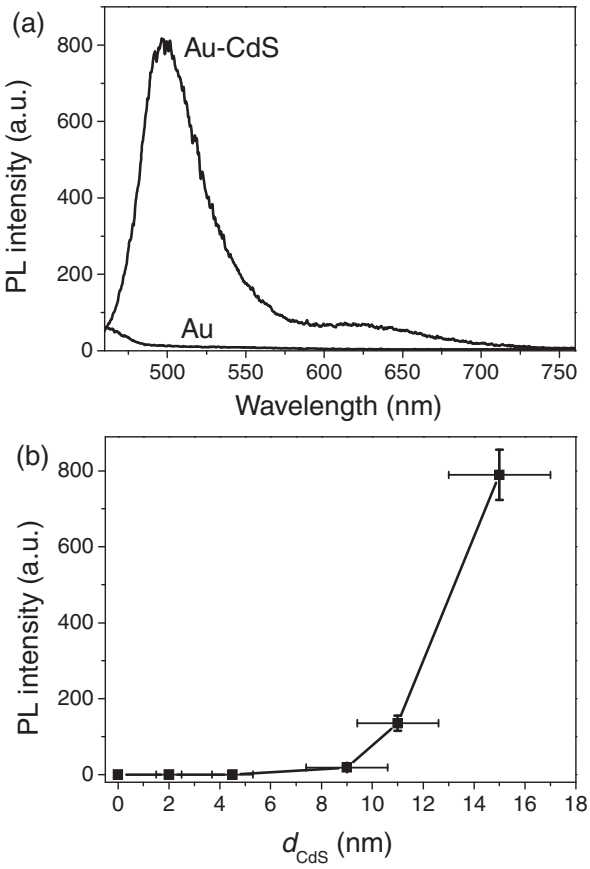

Figure 6. a) Emission spectra of Au nanorods and Au–CdS nanorods with d_{CdS} of 15.0 nm excited at 400 nm by using a CW light. b) PL intensity versus d_{CdS}.

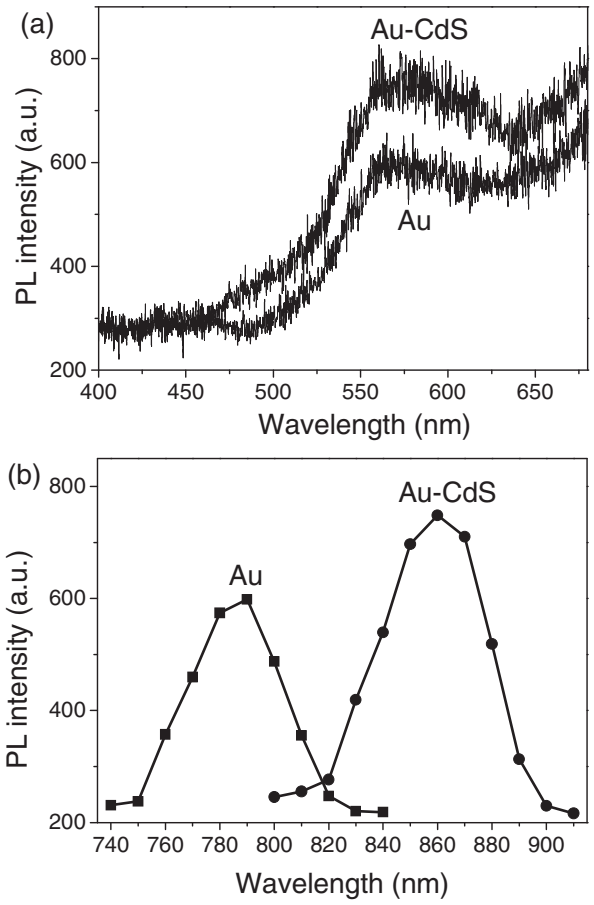

Figure 7. a) Two-photon PL spectra of Au nanorods (λ_{ex} = 790 nm) and Au–CdS nanorods (λ_{ex} = 860 nm). b) PL excitation spectra (λ_{em} = 580 nm) of Au nanorods and Au–CdS nanorods. All the samples are dispersed in water solution with the same gold molar concentration of 4.0 nM.

2.3. One-Photon Luminescence

The one-photon luminescence properties of the Au–CdS nanorods are shown in **Figure 6**. Under a 400-nm continuous wave (CW) light excitation, the Au–CdS nanorods with a CdS shell thickness d_{CdS} of about 15.0 nm show a narrow emission at around 498 nm along with a fainter and broader low-energy peak centered at around 640 nm, whereas the original Au nanorods show almost no luminescence. Such emission profiles are similar to the previously reported results for CdS nanorods: the 498 nm emission can be ascribed to direct electron-hole recombination (i.e., band-edge emission), and the 640 nm emission is due to trap-related electron-hole recombination of CdS.[47,48]

The emission intensity of the Au–CdS nanorods was lower than that of the free CdS nanoparticles synthesized without Au, which implies an emission quenching effect related to the coupling of excitons and plasmons in such core–shell structures.[25,49] As shown in Figure 6b, the Au–CdS nanorods with thinner CdS shells showed a greatly decreased PL intensity because of the decreased average distance between the Au and CdS components. Particularly for Au–CdS nanorods with d_{CdS} less than 9.0 nm, almost no emission could be observed. The corresponding emission dynamics were studied in detail by using a pulsed laser as the excitation source (see Figure S5 in the Supporting Information for details).[50,51] The coupling of excitons and plasmons is believed to enable the funneling of energy into the gold cores.[22]

2.4. Enhanced Two-Photon Luminescence

Figure 7 shows the two-photon PL properties of the Au nanorods (λ_{ex} = 790 nm) and Au–CdS nanorods (λ_{ex} = 860 nm), both of which were excited around their respective LSPR peaks. The Au and Au–CdS nanorods were dispersed in a water solution with the same gold molar concentration of about 4.0 nM. A Ti:sapphire laser was employed for excitation, and two 700-nm short wave pass filters were used to eliminate the laser scattering. The input pulse intensity was about 0.10 GW cm^{-2}, which was lower than the level used for two-photon imaging of gold nanorods (4–20 GW cm^{-2}), as reported recently.[38] The Au and Au–CdS nanorods showed emission spectra peaks at around 580 nm, which were similar to the two-photon PL spectra of the Au nanorods reported previously.[38] The spectral measurements were blocked around 700 nm because of the filter limitations of the measurement system. By measuring the dependence of the emission intensity on the excitation power, a quadratic dependence on the incident power of around

2.0 could be observed for increasing excitation powers, indicating that the excitation was a two-photon process (see Figure S6 in the Supporting Information). When the nanorods were excited at the same excitation power with the laser running in CW mode, the signal intensity was reduced to background noise levels, thus further confirming that the emission spectra were due to two-photon luminescence.

As shown in Figure 7a, the two-photon PL intensity of the Au–CdS nanorods was around 1.5 times that of the free Au nanorods when excited at the respective LSPR peak wavelengths. Such PL enhancement can probably be ascribed to the following mechanisms. Firstly, the Au–CdS nanorods with complete core–shell structures provide an efficient platform for exciton-plasmon interactions, which can result in the energy transfer from the CdS shells to the Au cores. When the Au–CdS nanorods are under NIR laser excitation, CdS can also be excited by two-photon excitation processes, in which case energy is transferred from the CdS shell to the nearby Au core (See Figure S7 in Supporting Information for such energy transfer scheme). Secondly, the tight field confinement, in other words the electromagnetic field enhancement, also contributes to such PL enhancement.[18–20] The metal-based core–shell nanostructures with high shell refractive index can support larger electromagnetic field enhancement in the cavity than the bare metal particles.[18] The shells, which have a higher refractive index than the medium, can confine the light in such structures. Such electromagnetic field enhancement mechanism has been reported as the SERS enhancement seen in Ag-SiO_2 core–shell structures.[20] Furthermore, in our Au–CdS core–shell nanorods, the large electromagnetic field at the LSPR wavelength may also contribute to the CdS two-photon excitation mentioned above.

To further determine the relationship between the two-photon luminescence and the surface plasmonic mode, the dependence of the emission intensity on the excitation wavelength of the Au–CdS nanorods was measured (see Figure 7b). The excitation spectra of the Au and Au–CdS nanorods had peaks at 790 and 860 nm, respectively, which coincide with their respective LSPR peaks. These results confirm that the two-photon luminescence of the Au–CdS nanorods is also governed by the electromagnetic field enhancement from the plasmon resonance. Similar excitation profiles for gold nanorods have been observed by Wang et al.[36] The excitation spectrum near the plasmon resonance had a narrower bandwidth than the absorbance peak because of the nonlinear character of the two-photon luminescence.[36] The results suggest that the exciton-plasmon interactions in the Au–CdS nanorods can create new possibilities for enhancing and regulating the excitation profiles of Au two-photon luminescence.

3. Conclusions

The synthesis of Au–CdS hetero-nanorods with complete core–shell structures and controllable shell thickness was demonstrated. The Au–CdS nanorods obtained demonstrated tailored LSPR absorption features and Au-quenched exciton luminescence and they exhibited plasmon-governed and enhanced two-photon luminescence, which can be ascribed to the exciton-plasmon interactions. This approach is an efficient method to overcome the limitations of lattice mismatch and has potential for the preparation of various metal-semiconductor hetero-nanostructures. Furthermore, the synthesized Au–CdS nanorods showed efficient exciton-plasmon coupling, which can integrate the attractive optical properties of both metal and semiconductor components, and thus they are of special interest for many applications such as optical biosensors, two-photon imaging, photocatalysis, and functional optoelectronic devices.

4. Experimental Section

Chemicals: Chloroauric acid ($HAuCl_4{\cdot}4H_2O$, 99.99%), silver nitrate ($AgNO_3$, 99.8%), glycine acid (99.5%), sulfur powder (99.5%), L-ascorbic acid (99.7%), sodium hydrate (NaOH, 96.0%), cadmium nitride tetrahydrate ($Cd(NO_3)_2{\cdot}4H_2O$, 99.0%), hydrochloric acid (36–38%), and sodium borohydride ($NaBH_4$, 96%) were purchased from Sinopharm Chemical Reagent Co. Ltd (Shanghai, China). Hexadecyltrimethylammonium bromide (CTAB, 99.0%) was purchased from Amresco Inc. (America). All chemicals were used as received without further purification. All aqueous solutions were freshly prepared in double distilled water.

Synthesis of Gold Nanorods: The gold nanorods were prepared in aqueous solutions using a seed-mediated growth method.[43,44] Specifically, the gold seed solution was first prepared by the addition of 10 mL of 0.0005 M $HAuCl_4$ solution into 10 mL of 0.2 M CTAB. The solution was gently mixed. A freshly prepared, ice-cold $NaBH_4$ solution (1.2 mL, 0.01 M) was then injected dropwise into the mixture solution under vigorous shaking. To grow gold nanorods, 1.2 mL of 0.005 M $HAuCl_4$ and 0.012 mL of 0.1 M $AgNO_3$ were first mixed with 6 mL of 0.2 M CTAB. Then, 0.012 mL of 2.0 M HCl was added, followed by the addition of 0.66 mL of 0.1 M ascorbic acid. After the solution was mixed by inversion, different amounts of the CTAB-stabilized gold seed solution were rapidly injected. The resultant solution was gently mixed for 10 s and was left undisturbed overnight.

Synthesis of Au–CdS Core–Shell Nanorods: The original Au nanorod concentration in the growth solution was estimated to be about 8.0 nM according to previously measured extinction coefficients at the LSPR peak wavelength.[52] The method included three steps to obtain Au–Ag, Au–Ag_2S, and Au–CdS nanorods. Step 1: In a typical synthesis of Au–Ag nanorods, 1 mL of the synthesized Au nanorod solution was mixed with 1 mL of 0.2 M glycine acid and 0.03 mL of 2.0 M NaOH. After adding 2.5 μL of 0.1 M $AgNO_3$, the mixture was incubated at 32 °C without stirring for 10 h. Step 2: The Au–Ag_2S nanorods were prepared by mixing an excess amount of sulfur powder into the Au-Ag nanorod solution, and the mixture was kept at 32 °C overnight. The synthesized Au-Ag_2S nanorod solution was used directly to grow the Au–CdS nanorods. Step 3: To synthesize Au–CdS nanorods, different amounts of 0.1 M $Cd(NO_3)_2$ were added into the Au-Ag_2S solution, and the mixture was stirred for 30 min. Then, 0.1 mL of 0.01 M $NaBH_4$ solution was added dropwise into the mixture. The solution was kept at 50 °C and stirred for 30 min. The final product (Au–CdS core–shell nanorods) was centrifuged, washed, and dispersed in water.

Sample Characterization: Several drops of the water solution of each sample were placed on a carbon-coated copper grid and were dried under ambient conditions for TEM and HRTEM characterization. TEM and HRTEM observations were performed with a JEOL 2010 HT and a JEOL 2010 FET transmission electron microscope operated at 200 kV. EDX analysis was performed on an EDAX instrument incorporated in the HRTEM. The absorption spectra of the samples were measured using a TU-1810 UV-vis spectrophotometer (Purkinje General Instrument Co.Ltd. Beijing, China).

Optical Measurements: For one-photon PL measurements the fluorescence emission spectra were recorded using a Hitachi F-4500 fluorescence spectrophotometer with a Xe lamp as the excitation source. For two-photon PL measurements the excitation source was a mode-locked Ti:sapphire laser (Mira 900, Coherent) with a pulse width of

around 3 ps and a repetition rate of 76 MHz. The PL from the sample was collected by the focusing lens and filtered by a 700-nm short-wave pass filter before entering the spectrometer detector. The PL spectra were recorded by a spectrometer (Spectrapro 2500i, Acton) with a liquid-nitrogen cooled CCD (SPEC-10: 100B, Princeton). The Au and Au–CdS samples in the PL measurements were prepared using the procedure described below. The original Au nanorods were divided equally into two parts: Part A and Part B. Part A was directly centrifuged and dispersed in 2 mL of water. Their molar concentration was estimated to be about 4.0 nM according to the measured extinction coefficients at the LSPR peak wavelength.[52] Part B was used to synthesize Au–CdS nanorods and the final products were centrifuged and dispersed in another 2 mL of water. The samples of Part A and Part B were used as the Au and Au–CdS samples for comparing the PL intensity.

Supporting Information

Supporting Information is available from the Wiley Online Library or from the author.

Acknowledgements

This work was supported by the NSFC (10874134 and 10904119), the National Program on Key Science Research of China (2011CB922201), and the Key Project of the Ministry of Education of China (708063).

Received: October 22, 2010
Revised: December 9, 2010
Published online: March 22, 2011

[1] J. Lee, P. Hernandez, J. Lee, A. O. Govorov, N. A. Kotov, *Nat. Mater.* **2007**, *6*, 291.
[2] Y. Jin, X. Gao, *Nat. Nanotechnol.* **2009**, *4*, 571.
[3] J. Zhang, Y. Tang, K. Lee, M. Ouyang, *Nature* **2010**, *466*, 91.
[4] A. Dawson, P. V. Kamat, *J. Phys. Chem. B* **2001**, *105*, 960.
[5] H. Y. Lin, Y. F. Chen, J. G. Wu, D. I. Wang, C. C. Chen, *Appl. Phys. Lett.* **2006**, *88*, 161911.
[6] G. H. Ma, J. He, K. Rajiv, S. H. Tang, Y. Yang, M. Nogami, *Appl. Phys. Lett.* **2004**, *84*, 4684.
[7] J. Lee, A. O. Govorov, J. Dulka, N. A. Kotov, *Nano Lett.* **2004**, *4*, 2323.
[8] Z. Sun, Z. Yang, J. Zhou, M. H. Yeung, W Ni, H. Wu, J. Wang, *Angew. Chem. Int. Ed.* **2009**, *48*, 2881.
[9] R. Costi, A. E. Saunders, E. Elmalem, A. Salant, U. Banin, *Nano Lett.* **2008**, *8*, 637.
[10] E. Formo, E. Lee, D. Campbell, Y. N. Xia, *Nano Lett.* **2008**, *8*, 668.
[11] J.-S. Lee, E. V. Shevchenko, D. V. Talapin, *J. Am. Chem. Soc.* **2008**, *130*, 9673.
[12] H. M. Gong, X. H. Wang, Y. M. Du, Q. Q. Wang, *J. Chem. Phys.* **2006**, *125*, 024707.
[13] N. G. Liu, B. S. Prall, V. I. Klimov, *J. Am. Chem. Soc.* **2006**, *128*, 15362.
[14] T. Mokari, E. Rothenberg, I. Popov, R. Costi, U. Banin, *Science* **2004**, *304*, 1787.
[15] A. V. Akimov, A. Mukherjee, C. L. Yu, D. E. Chang, A. S. Zibrov, P. R. Hemmer, H. Park, M. D. Lukin, *Nature* **2007**, *450*, 402.
[16] Z. K. Zhou, M. Li, Z. J. Yang, X. N. Peng, X. R. Su, Z. S. Zhang, J. B. Li, N. C. Kim, X. F. Yu, L. Zhou, Z. H. Hao, Q. Q. Wang, *ACS Nano* **2010,***4*, 5003.
[17] J. Yang, H. I. Elim, Q. Zhang, J. Y. Lee, W. Ji, *J. Am. Chem. Soc.* **2006**, *128*, 11921.
[18] H. Xu. *Appl. Phys. Lett.* **2004** , *85*, 5980.
[19] H. Xu. *Phys. Rev. B* **2005** , *72*, 073405.
[20] W. Wang, Z. Li, B. Gu, Z. Zhang, H. Xu. *ACS Nano* **2009** , *3*, 3493.
[21] H. Wei, D. Ratchford, X. Li, H. Xu, C.-K. Shi, *Nano Lett.* **2009**, *9*, 4168.
[22] Y. Fedutik, V.V. Temnov, O. Schps, U. Woggon, M. V. Artemyev. *Phys. Rev. Lett.* **2007**, *99*, 136802.
[23] W. Shi, H. Zeng, Y. Sahoo, T. Y. Ohulchanskyy, Y. Ding, Z. L. Wang, M. Swihart, P. N. Prasad, *Nano Lett.* **2006**, *6*, 875.
[24] C. H. Kuo, T. E. Hua, M. H. Huang, *J. Am. Chem. Soc.* **2009**, *131*, 17871.
[25] W. T. Chen, T. T. Yang, Y. J. Hsu, *Chem. Mater.* **2008**, *20*, 7204.
[26] J. Zhang, Y. Tang, K. Lee, M. Ouyang, *Science* **2010**, *327*, 1634.
[27] J. Yang, E. H. Sargent, S. O. Kelley, J. Y. Ying, *Nat. Mater.* **2009**, *8*, 683.
[28] J. Zeng, J. Huang, C. Liu, C. H. Wu, Y. Lin, X. Wang, S. Zhang, J. Hou, Y. Xia, *Adv. Mater.* **2010**, *22*, 1936.
[29] F. R. Fan, Y. Ding, D. Y. Liu, Z. Q. Tian, Z. L. Wang, *J. Am. Chem. Soc.* **2009**, *131*, 12036.
[30] L. Wang, R. Yan, Z. Huo, L. Wang, J. Zeng, J. Bao, X. Wang, Q. Peng, Y. Li, *Angew. Chem. Int. Ed.* **2005**, *44*, 6054.
[31] Z. H. Bao, Z. H. Sun, M. D. Xiao, L. W. Tian, J. F. Wang, *Nanoscale* **2010**, *2*, 1650.
[32] R. D. Robinson, B. Sadtler, D. O. Demchenko, C. K. Erdonmez, L. W. Wang, A. P. Alivisatos, *Science* **2007**, *317*, 355.
[33] T. K. Sau, A. L. Rogach, *Adv. Mater.* **2010**, *22*, 1781.
[34] X. Huang, S. Neretina, M. A. El-Sayed, *Adv. Mater.* **2009**, *21*, 4880.
[35] C. Wang, Z. Ma, T. Wang, Z. Su, *Adv. Funct. Mater.* **2006**, *16*, 1673.
[36] H. Wang, T. B. Huff, D. A. Zweifel, W. He, P. S. Low, A. Wei, J. X. Cheng, *Proc. Natl. Acad. Sci. USA* **2005**, *102*, 15752.
[37] N. J. Durr, T. Larson, D. K. Smith, B. A. Korgel, K. Sokolov, A. Ben-Yakar, *Nano Lett.* **2007**, *7*, 941.
[38] J. Zhu, K.-T. Yong, I. Roy, R. Hu, H. Ding, L. Zhao, M. T. Swihart, G. S. He, Y. Cui, P. N. Prasad, *Nanotechnology* **2010**, *21*, 285106.
[39] X. Wu, T. Ming, X. Wang, P. N. Wang, J. F. Wang, J. Y. Chen, *ACS Nano* **2010**, *4*, 113.
[40] K. Imura, T. Nagahara, H. Okamoto, *J. Phys. Chem. B* **2005**, *109*, 13214.
[41] P. Matteini, F. Ratto, F. Rossi, S. Centi, L. Dei, R. Pini, *Adv. Mater.* **2010**, *22*, 4313.
[42] Y. Y. Yu, S. S. Chang, C. L. Lee, C. R. C. Wang, *J. Phys. Chem. B* **1997**, *101*, 6661.
[43] N. R. Jana, L. Gearheart, C. J. Murphy, *J. Phys. Chem. B* **2001**, *105*, 4065.
[44] I. Pastoriza-Santos, J. Pérez-Juste, L. M. Liz-Marzán, *Chem. Mater.* **2006**, *18*, 2465.
[45] M. Li, Z. S. Zhang, X. Zhang, K. Y. Li, X. F. Yu, *Opt. Express* **2008**, *16*, 14288.
[46] M. Liu, P. Guyot-Sionnest. *J. Phys. Chem. B* **2004** , *108*, 5882.
[47] Z. Zhuang, X. Lu, Q. Peng, Y. Li, *J. Am. Chem. Soc.* **2010**, *132*, 1819.
[48] A. E. Saunders, A. Ghezelbash, P. Sood, B. A. Korgel, *Langmuir* **2008**, *24*, 9043.
[49] A. Agarwal, G. D. Lilly, A. O. Govorov, N. A. Kotov, *J. Phys. Chem. C* **2008**, *112*, 18314.
[50] T. Uchihara, H. Kato, E. Miyagi, *J. Photochem. Photobiol. A: Chem.* **2006**, *181*, 86.
[51] V. Klimov, P. H. Bolivar, H. Kurz, *Phys. Rev. B* **1996**, *53*, 1463.
[52] C. J. Orendorff, C. J. Murphy, *J. Phys. Chem. B* **2006**, *110*, 3990.